Infrared Spectra of the Complexes of Trifluoroethene with Dimethyl Ether, Acetone, and Oxirane: A Cryosolution Study

Wouter A. Herrebout, Sofie N. Delanoye, Bert U. W. Maes, and Benjamin J. van der Veken*,†

Contribution from the Department of Chemistry, University of Antwerp, Groenenborgerlaan 171, B2020 Antwerp, Belgium

Received: August 25, 2006

Infrared spectra of solutions of trifluoroethene and dimethyl ether, acetone, or oxirane in liquid krypton and liquid argon have been studied. For each Lewis base the formation of a 1:1 complex with the Lewis acid was observed. The C−H stretching of trifluoroethene being perturbed by a strong Fermi resonance, the complexes with trifuloroethene-*d* were also investigated and showed that in each case the hydrogen bond between the acid and base is of the traditional, red-shifting type. The structures of the complexes were investigated using ab initio calculations. These indicate that with dimethyl ether and acetone two different isomeres can be formed, but with a single one detected in the solution in each case. The Fermi resonance in the complex with unlabeled trifluoroethene is discussed using data derived form ab initio potential and dipole hypersurface calculations. The complexation enthalpies of the complexes were obtained from temperature dependent studies of the solutions and are discussed in relation to the ab initio complexation energies and Monte Carlo free energy perturbation calculations of solvent effects.

Introduction

In recent years an increasing number of C−H···O hydrogen bonds has been documented, both theoretically and experimentally.[1−11] It was thereby found that the hydrogen bond formed by a C(sp^3)−H bond can be of the blue-shifting type when strongly electronegative substituents are present on the same carbon atom. This type of hydrogen bond is characterized by a shortening of the C−H bond distance and a shift toward higher wavenumbers of the C−H stretching frequency.[12] The blue-shifting phenomenon has been observed for complexes of Lewis acids such as F_3CH, F_2ClCH, and FCl_2CH with Lewis bases containing an oxygen donor atom such as dimethyl ether, acetone and oxirane.[13−17] Far less is known about the complexing capabilities of C(sp^2)−H bonds, and data on blue-shifting hydrogen bonding in that type of hydrogen donors appear to lack altogether. In view of the above restriction, the most likely candidate for blue shifting would be trifluoroethene, $F_2C{=}CFH$ (TFE). Complexes of, among others, this Lewis acid with dimethyl ether and acetone were detected in the co-deposition matrix isolation infrared spectra.[18] The authors list surprisingly large red shifts of −76 and −70 cm^{-1} for the $\nu_1^{C_2F_3H}$ in the complexes with dimethyl ether and acetone, respectively. The value for the dimethyl ether complex appears not to be supported by more recent ab initio results[19] reported on the complex of the same Lewis acid with the similar Lewis base H_2O, where a much smaller (harmonic) red shift of 16 cm^{-1} is predicted. Closer scrutiny of the matrix isolation data[18] shows that the authors have not considered the strong Fermi resonance by which $\nu_1^{C_2F_3H}$ in the monomer is disturbed.[20,21] It also cannot be deduced from their published data if the Fermi resonance persists in the complex: a change in that resonance would certainly contribute to the observed shift, so that the uncorrected result no longer reflects the strength nor the type of the hydrogen bonding. The trifluoroethene/dimethyl ether complex has also been studied using FT microwave spectroscopy.[22] The structure refined from the rotational constants confirms the presence of a hydrogen bond between the ethene C−H bond and the oxygen atom, but more intricate properties of the hydrogen bond, such as the (small) change in the ethene C−H bond length, were not reported. It is, therefore, clear that, even when the formation of a complex has been substantiated, the type and strength of the hydrogen bonding interaction remain to be properly described.

To expand our understanding of the complex-forming characteristics of trifluoroethene in general, and to accurately describe the hydrogen bonding type that is present in these complexes, we have studied, using infrared spectroscopy, the formation of complexes of the said Lewis acid with dimethyl ether (DME), acetone (AC), and oxirane (OX). The complexes were studied in liquid rare gases, and the experimental data were interpreted with the help of ab initio calculations on structures and harmonic and anharmonic vibrational frequencies, and with the help of Monte Carlo calculations to describe the solvent influences on the stabilities of the complexes.

Experimental Section

Synthesis. Samples of DME (99+%), DME-d_6 (98 at. %), AC (99+%), AC-d_6, (99.5 at. %) OX (98+%), OX-d_4 (98 atom %), and TFE (98+%) were purchased from Sigma Aldrich, Isotec, and ABCR. The compounds were used as obtained.

A sample of TFE-d_1 was synthesized using the (trifluoroethenyl)cadmium reagent, which was prepared by reaction of iodotrifluoroethene with cadmium powder.[23] The reaction was excecuted on a vacuum manifold. In a first step, 25 mmol of cadmium powder were placed in a sample tube and degassed on the manifold for 24 h. Subsequently, 4 mL of dry dimethylformamide were added via a vacuum addition funnel, the resulting mixture was cooled with liquid nitrogen (LN_2), and 4 mmol of C_2F_3I was distilled. The liquid nitrogen dewar used to cool the mixture was then replaced by a 2-propanol/LN_2 slush,

† E-mail: benjamin.vanderveken@ua.ac.be.

10.1021/jp065502z CCC: $33.50
Published on Web 12/02/2006

which was allowed to slowly warm to 0° C, after which the mixture was stirred for 1 h. Next, any unreacted C_2F_3I was pumped off, the remaining mixture was cooled to LN_2 temperature, and in a single batch 100 mmol of D_2O was distilled. Upon warming, a vigorous reaction took place, indicating hydrolysis of the organocadmium reagent. This reaction is characterized by a kinetic isotope effect, causing the HOD impurity in the D_2O to react significantly faster than D_2O itself. As a result, the product gas formed in the first couple of minutes of the reaction was found to contain notable amounts of unlabeled TFE: this batch was discarded. The subsequently collected gas was observed to be nearly free of unlabeled TFE.

Vibrational Spectroscopy. Infrared spectra were recorded on a Bruker IFS 66v Fourier transform spectrometer. For the mid-IR, a Globar source was used in combination with a Ge/KBr beam splitter and a broad band LN_2-cooled MCT detector. For the far-IR, a 6 μm Mylar beam splitter was used in combination with a LHe-cooled Si bolometer. For the near-IR a CaF_2 beam splitter was used in combination with a LN_2-cooled InSb detector. The interferograms were averaged over 500 (mid-IR), 1500 (far-IR), and 5000 (near-IR) scans, Blackmann−Harris three-term apodized and Fourier transformed with a zero filling factor of 4, to yield spectra with a resolution of 0.5 cm^{-1}.

The experimental setup used to investigate the solutions in liquid noble gases has been described in detail before.[24] Liquid cells with path lengths of 0.06, 1.0, 4.0, and 7.0 cm, equipped with wedged silicon or CaF_2, were used to record the spectra.

Ab Initio Calculations. Geometries and vibrational frequencies of monomers and complexes were obtained at the MP2/6-31++G(d,p) level. During all calculations, corrections for BSSE were accounted for using CP-corrected gradient techniques.[25] Complexation energies were derived by subtracting the monomer energies from that of the complex. For all monomeric species, cubic and quartic force constants were calculated using the finite difference approach.[26] Calculations were performed using Gaussian03/TCP Linda,[27] installed on local workstations and on the CalcUA computer cluster.

Single point calculations were performed at the MP2/aug-cc-PVXZ (with X = D, T and Q level), using the MP2/6-31++G(d,p) geometries. For these, the Local-MP2 approximation[28] implemented in the parallel-PQS software package was used.[29] The number of processors used was varied from 8 to 32, whereas the parallelization was enabled using the Parallel Virtual Machine environment. To reduce numerical errors, the integral thresholds in the SCF and MP2 calculations were set to 10^{-14}.

The topology of the electron density was investigated using the Atoms in Molecules (AIM) approach, using AIM2000.[30]

Monte Carlo Simulations. Solvation Gibbs energies were obtained from Monte Carlo calculations, using a modified version of BOSS 4.1,[31] as described before.[32] The enthalpy of solvation $\Delta_{sol}H$ and the entropy of solvation $\Delta_{sol}S$ in LAr and LKr were extracted from the Gibbs energies of solvation $\Delta_{sol}G$, using the expressions $\Delta_{sol}S = -\partial(\Delta_{sol}G)/\partial T$ and $\Delta_{sol}H = \Delta_{sol}G + T\Delta_{sol}S$. To this end, Gibbs energies of solvation were calculated at 11 different temperatures between 88 and 138 K for LAr, and between 120 and 175 K for LKr, at a pressure of 28 bar, i.e., the vapor pressure of LAr and LKr at the highest temperatures studied.

Results

Ab Initio Calculations. Geometry optimizations of the complexes were performed starting from different relative positions of TFE and the Lewis bases. The resulting structures and the predicted changes in the CH bond length are collected in Figure 1.

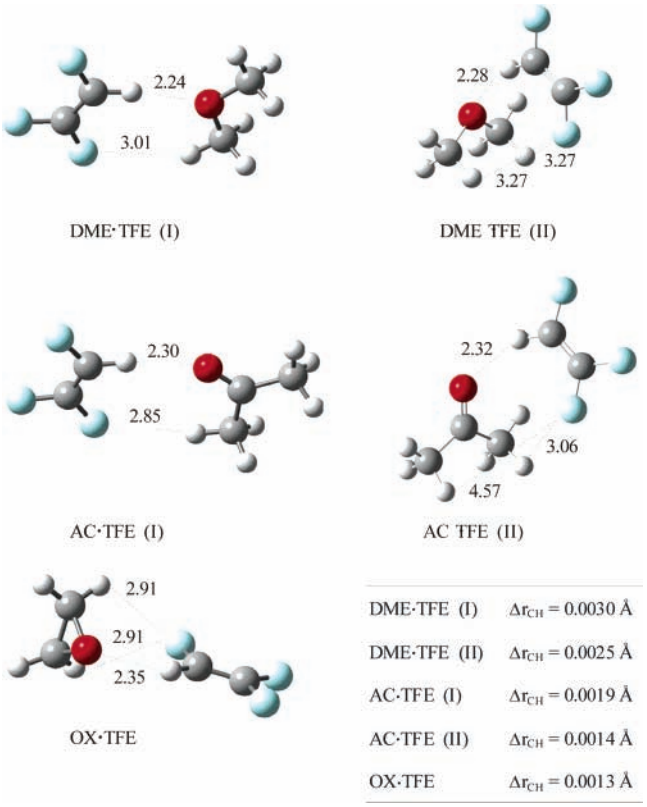

Figure 1. Ab initio structures of the complexes of trifluoroethene with dimethyl ether, acetone, and oxirane.

For TFE·DME, the calculations converged to two minima, each with C_s symmetry. In the first isomer, DME·TFE (I), the TFE moiety is situated in the heavy atom plane of DME. This isomer has a CH···O hydrogen bond with a bond length of 2.24 Å, and a secondary interaction involves a C−F bond and one of the antiperiplanar C−H bonds in DME, the F···H interatomic distance being approximately 3.01 Å. In the second isomer, DME·TFE (II), the TFE moiety is situated in the plane that passes through the DME oxygen atom and that is perpendicular to the DME heavy atom plane. The interaction occurs through a CH···O hydrogen bond and through two weaker interactions, involving a single fluorine atom and two synclinal hydrogen atoms located on the same side of DME.

The geometry derived from a combined microwave/ab initio study[22] has the structure of isomer II. The reported H···O and the F···H interatomic distances are 2.33(25) (microwave) and 2.31 Å (ab initio) and 2.71(45) (microwave) and 2.79 Å (ab initio), respectively. The ab initio results in that study[22] describe only the perpendicular isomer II. Our calculations, however, show that also at the level used in that study the planar isomer I is a local minimum.

The AIM analysis for TFE·DME (I) reveals the presence of two bond critical points between the monomers, corresponding to CH···O and the CH···F hydrogen bonds. For isomer II a single bond critical point is present, in the CH···O hydrogen bond. This suggests that the secondary interactions in II are too weak to be classified as C−H···F hydrogen bonds and must rather be classified as weak electrostatic interactions.

Also for TFE·AC two different isomers were found. In the more stable AC·TFE (I), the TFE moiety is situated in the heavy atom plane of AC, the two interacting via a relatively strong

TABLE 1: MP2=FULL Complexation Energies and Complete Basis Set Limits, in kJ mol^{-1}, for the Complexes of TFE with DME, AC En OX

	6-31++ G(d,p)	aug-cc-PVDZ[a]	aug-cc-PVTZ[a]	aug-cc-PVQZ[a]	limit[b]
TFE·DME(I)	−15.1	−14.9	−16.1	−16.6	−17.1(1)
TFE·DME(II)	−14.4	−14.8	−15.9	−16.5	−17.0(1)
TFE·AC(I)	−14.8	−15.8	−16.9	−17.4	−17.9(2)
TFE·AC(II)	−14.6	−15.5	−16.5	−16.9	−17.4(1)
TFE·OX	−15.2	−15.7	−16.8	−17.3	−17.9(1)

[a] Single point energies using MP2/6-31++G(d,p) equilibrium geometries. [b] Complete basis set limit derived from the aug-cc-PVXZ (X = D, T, and Q) calculations.

CH···O hydrogen bond and a weaker, secondary interaction involving a fluorine atom of the TFE and a hydrogen atom of AC. The second isomer, AC·TFE (II), has the TFE molecule tilted away from the AC heavy atom plane. Also for this structure secondary F···H interactions occur via F···H distances that are close to 3.06 and 4.57 Å. A single bond critical point is found in the region of the shortest distance. It follows that only for that distance a C−F···H hydrogen bond is formed.

For OX only a single complex with TFE was found. The equilibrium geometry has C_s symmetry, and the relative orientation of the two molecules is analogous to the one in TFE·DME(II). For the OX complex, however, bond critical points are found for the hydrogen bond and for the two F···H interactions, showing that the latter are stronger than in TFE·DME(II).

The structural data in Figure 1 indicate that the C−H(···O) bonds are slightly elongated in the complexes, by amounts between +0.0013 and +0.0030 Å. This weakening is in line with the red shifts, between −10 and −30 cm^{-1}, predicted for the $\nu_1^{C_2F_3H}$ (vide infra).

The MP2/6-31++G(d,p) complexation energies derived from the CP-corrected PES are collected in Table 1. All values can be seen to be close to 15 kJ mol^{-1}. To account for the effect of the size of the basis set, additional single point calculations were performed at the MP2/aug-cc-PVDZ, MP2/aug-cc-PVTZ, and MP2/aug-cc-PVQZ levels, using the equilibrium geometries obtained with the 6-31++G(d,p) basis set, and the complete basis set limit was obtained by plotting the complexation energies for the aug-cc-PVXZ (X = D, T, and Q) levels as a function of 1/n, in which n is the number of basis functions. The resulting single point energies and basis set limits, obtained by extrapolating the energies toward an infinite basis set, are also given in Table 1.

Table 1 shows that the complexation energies have similar values for all Lewis bases, varying between −17.0 kJ mol^{-1} for DME·TFE (II) and −17.9 kJ mol^{-1} for AC·TFE (I) and OX·TFE. It can further be seen that for the DME complexes the energy difference between isomers I and II is a mere 0.1 kJ mol^{-1}, whereas for the AC complexes isomer I is slightly more stable, by approximately 0.6 kJ mol^{-1}, than isomer II.

Monomer Spectra. The vibrational spectra of DME, AC, and OX dissolved in LAr and LKr have been studied before; the assignments have been well established and need no further comment.[13−15,33,34] The infrared and Raman spectra of TFE and TFE-d_1 have been described by Mann.[20] The more important frequencies observed for the vapor phase by these authors are compared with the present values in LAr and LKr and with the ab initio values in Table 2. Comparison shows that for most fundamentals the agreement between experimental and theoretical values is excellent.

It has been observed [20] that the C−H stretching fundamental, ν_1, is perturbed by a Fermi resonance involving also the $\nu_2 + \nu_3$ combination level. The resonance persists in the rare gas solutions, giving rise to a doublet with maxima at 3158.0 and 3110.8 cm^{-1} in LAr, and at 3155.2 and 3107.9 cm^{-1} in LKr.

On the low-frequency side of the 1171 cm^{-1} $\nu_4(a')$ P,Q,R structure in the gas-phase spectrum of TFE a shoulder near 1153 cm^{-1} was assigned as $\nu_6 + \nu_9$.[20] In the spectrum of the LAr solution in this region two prominent bands, at 1169.6 and 1152.3 cm^{-1}, are found. Their full widths at half-height are between 3 and 4 cm^{-1}, so they are well separated, and their intensity can be accurately established from a least squares band fitting. The results of such a fit indicate that the 1152.3 cm^{-1} band is some 15% more intense than the 1169.6 cm^{-1} band, and some 30% more intense than ν_6 at 927.2 cm^{-1}. As ν_9 has a very low infrared intensity, it is rather unlikely that the $\nu_6 + \nu_9$ combination band should be more intense than ν_6 itself. Hence, the intensities in the 1169.6/1152.3 cm^{-1} doublet suggest that the ν_5 and $\nu_6 + \nu_9$ levels are perturbed by the Fermi resonance. Evidence supporting this is the value of the cubic force constant α_{469}. Assuming that the relative intensity of the unperturbed combination band may be neglected in comparison with that of ν_5, the absolute value of this constant is found to have the relatively large absolute value of 23.2 cm^{-1}, in excellent agreement with the ab initio value, obtained as described above, of −23.6 cm^{-1}. A further argument supporting the Fermi resonance was found by comparing normalized ab initio intensities with normalized experimental band areas. Normalization of the ab initio intensities was performed by the sum of the predicted infrared intensities of the transitions involved, whereas the experimental normalization constant was the sum of the corresponding band areas, for ν_5 using the complete 1169.6/1152.3 cm^{-1} doublet. The normalized band areas were

TABLE 2: Experimental Frequencies ($\Delta\bar{\nu}$, in cm^{-1}) and Experimental and ab Initio Complexation Shifts (in cm^{-1}) for Modes Localized in Trifluoroethene

		DME-d_6				AC-d_6			OX-d_4	
assignment	monomer[a]	LKr[b]	LAr[c]	I[d,f]	II[d,f]	LKr[b]	I[d]	II[d]	LKr[b]	I[d]
ν_{high}[e]	3155.2	−5.8	−5.6	(−35.0)	(−29.3)	−3.6	(−15.6)	(−10.3)	−4.5	(−10.8)
ν_{low}[e]	3107.9	−19.2	−20.1			−13.7			−13.8	
ν_2 (A′)	1784.4	−0.9	−0.3	−2.4	−5.0		−3.6	−3.9	−0.8	−3.6
ν_3 (A′)	1353.3	0.5	0.3	18.1	5.3	0.1	6.0	3.8	−0.1	−9.4
ν_4 (A′)	1261.4	2.1	2.5	−0.7	−6.3	−7.7	−6.7	−8.9	−2.6	−2.3
ν_5 (A′)	1168.5	−1.1	−0.1	−8.4	−11.3	−0.8	−9.1	−8.4	−0.4	−10.4
ν_6 (A′)	928.7	−1.4	−0.3	−3.8	−3.5		−4.1	−3.9	−5.5	−4.9
ν_{10} (A″)	750.1	48.1	52.4	60.6	75.5	42.6	65.1	54.0	40.5	55.0
ν_8 (A′)	484.8	0.0	−0.1	−0.3	−0.9	−0.3	−0.9	−1.1	−0.1	0.5

[a] Observed frequencies in liquid krypton. [b] Complexation shift observed in liquid krypton. [c] Complexation shift observed in liquid argon. [d] Complexation shifts derived from the MP2/6-31++G(d,p) potential energy surface. Roman numerals refer to the ab initio isomers of the complex. [e] ν_{high} and ν_{low} are the components of the C−H stretching Fermi doublet. [f] The shifts given in parentheses refer to the harmonic C−H stretch and cannot be directly compared with the shifts observed for the Fermi doublet.

TABLE 3: Observed Frequencies and Complexation Shifts, in cm^{-1}, for the Lewis Bases DME-d_6, AC-d_6 and OX-d_4 in Their 1:1 Complexes with TFE

assignment	$\bar{\nu}$/cm^{-1} monomer	complexation shift/cm^{-1} LKr[a]	I[b]	II[b]
		TFE·DME		
		CD stretch region		
	2293.2	−8.2		
$\nu_1(A_1)/\nu_{16}(B_2)$	2243.5	3.2	1.6/1.6	3.2/3.1
$\nu_{12}(B_1)$	2180.0	7.9	11.7	11.7
$\nu_2(A_1)$	2054.1	4.2	5.6	5.6
$\nu_{17}(B_2)$	2049.6	4.7	6.7	6.9
		fingerprint region		
$\nu_{13}(B_1)$	1060.8	0.4	−0.2	0.1
$\nu_{20}(B_2)$	1057.7	0.4	0.1	0.4
$\nu_5(A_1)$	1050.7	1.7	2.4	4.0
$\nu_6(A_1)$	826.4	−2.6	−3.8	−3.0
		TFE·AC		
$\nu_{20}(B_2)$	2259.0	2.4	1.9	0.8
$\nu_2(A_1)$	2220.0	2.0	0.9	1.7
$\nu_3(A_1)$	1732.6	1.3	−0.2	0.1
$\nu_{15} + \nu_{19}(A_1)$[b]	1709.8	−1.7		
$\nu_{21}(A_1)$	1047.5	−0.9	0.1	−0.6
$\nu_5(A_1)$	1033.8	−0.9	2.5	−0.6
$\nu_{17}(B_1)$	1002.1	2.1	1.7	1.9
$\nu_{19}(B_1)$	475.7	1.5	1.4	2.1
		TFE·OX		
$\nu_{13}(B_2)$	2314.1	5.1	6.0	
$\nu_1(A_1)$	2204.3	2.6	3.8	
$\nu_9(B_1)$	2171.3	3.7	4.1	
$\nu_2(A_1)$	1307.3	−1.2	−2.6	
$\nu_3(A_1)$	1011.7	1.0	0.8	
$\nu_4(A_1)$	962.3	−2.7	−4.4	
$\nu_{14}(B_2)$	895.0	0.6	1.1	
$\nu_{12}(B_1)$	804.3	−5.9	−6.7	
$\nu_5(A_1)$	751.7	1.1	3.9	

[a] Experimental complexation shifts, in liquid krypton. [b] Predicted complexation shifts. Roman numerals refer to the ab initio isomers of the complex.

found to vary by between 10 and 33% from their ab initio intensity, which is judged to be reasonable. The exception is the band area of the 1169.6 cm^{-1} band, which is smaller than the ab initio intensity by 125%. However, when the band area of the 1152.3 cm^{-1} band is added to that of the 1169.6 cm^{-1} band, the discrepancy is reduced to 5%. Thus, agreement of experiment with calculation of a level similar to that found for the other fundamentals is obtained for ν_5 only when it is assumed that its band area is repartitioned over the 1169.6/1152.3 cm^{-1} doublet: such a repartition is exactly what must be expected as the consequence of a $\nu_5/\nu_6 + \nu_9$ Fermi resonance.

Spectra of the Complexes. Infrared spectra of series of mixtures in LAr and in LKr containing mole fractions of DME-(-d_6), AC(-d_6), and OX(-d_4) ranging from 0.4×10^{-4} to 4.2×10^{-4} and containing TFE(-d_1) with mole fractions between 0.2×10^{-4} and 3.2×10^{-4} were investigated. New bands were observed in the spectra of the mixed solutions, which we assign to 1:1 complexes with TFE. The frequencies observed for the complexes with TFE, and their complexation shifts, are collected in Tables 2 and 3.

To avoid excessive overlap in the C−H stretching region, the complexes of unlabeled TFE were studied using fully deuterated Lewis bases. In Figure 2, the C−H stretching regions of spectra recorded at different temperatures from solutions in LKr that contain mole fractions of 1.3×10^{-4} of DME-d_6 and 6.0×10^{-4} of TFE (A), 8.9×10^{-5} of AC-d_6 and 7.3×10^{-4} of TFE (B), and 3.4×10^{-4} of OX-d_4 and 8.5×10^{-4} of TFE (C) are compared with those of solutions containing only DME-d_6, AC-d_4, OX-d_4, or TFE. Although significantly overlapped by monomer bands, new bands due to the complexes with DME-d_6, AC-d_4, and OX-d_4 can be observed. The spectra of the complexes were isolated from those of the monomers by subtracting out monomer contributions, using monomer spectra recorded at identical temperatures. The difference spectra are given as the lowest trace in each panel.

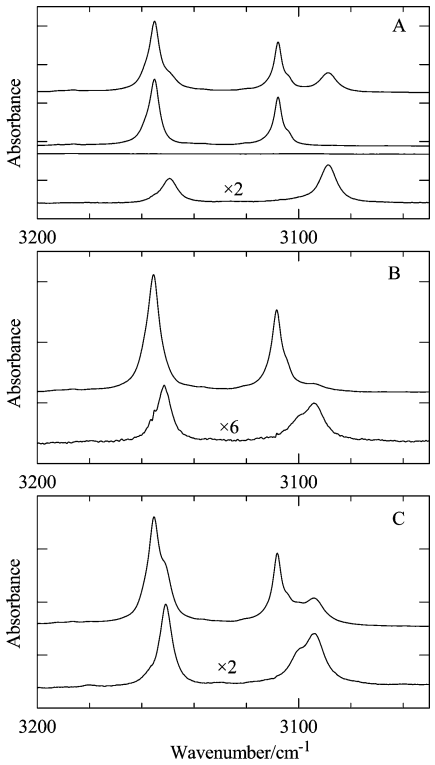

Figure 2. C−H stretching region of solutions in liquid krypton of trifluoroethene with dimethyl ether-d_6 (A) at 123 K, acetone-d_6 (B) at 149 K, and oxirane-d_4 (C), at 129 K. In panel A the traces are, from top to bottom, the spectrum of a mixture of TFE and DME-d_6, of a solution of DME-d_6, and of the complex in solution as obtained by subtracting the monomer spectra from that of the mixture. In panels B and C the top trace is the spectrum of the mixture and the lower trace is the spectrum of the complex. The ordinate tick mark interval in all panels equals 0.5 absorbance units. The spectra have been shifted vertically for clarity.

The complex of TFE with each of the Lewis bases gives rise to two prominent bands in the C−H stretching region, as is clear from Figure 2. Because a doublet is observed for TFE·OX-d_4, it is unlikely that the doublet structure is due to the presence of two isomers. Therefore, the doublets show that the Fermi resonance persists in the complexes. The results for the TFE-d_1 complexes, discussed in a following paragraph, support this conclusion.

With the above observations it becomes clear that the anomalous complexation shifts reported in the matrix isolation study[18] cannot be correct. For instance, for the DME complex in LAr the frequency difference between the monomer high-frequency component of the Fermi dyad and the low-frequency component of the complex is −67.3 cm^{-1}, rather close to the reported matrix shift of −76 cm^{-1}. Hence, it appears that in the matrix study the high-frequency component of the complex dyad remained unidentified.

It can be seen in Figure 2 that the low-frequency component of the Fermi dyad in monomer TFE has a low-frequency shoulder, near 3100 cm^{-1}. This band cannot be assigned as a first overtone nor as a binary combination band, and therefore, it cannot be in Fermi resonance with the C−H stretch. We

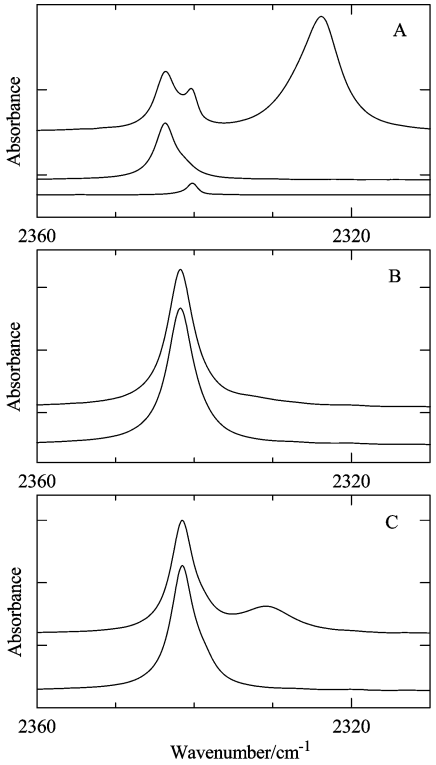

Figure 3. C−D stretching region of mixtures of trifluoroethene-d_1 with dimethyl ether (A) in liquid argon at 95 K, with acetone (B) in liquid krypton at 143 K, and with oxirane (C) in liquid krypton at 128 K. In panel A the traces are, from top to bottom, the spectrum of a mixture of TFE-d_1 and DME, of a solution of TFE-d_1, and of a solution of DME. In panels B and C the top trace is the spectrum of the mixture and the lower trace is the spectrum of a solution of TFE-d_1. The solutions of the respective Lewis bases show no bands in this region and are not given. The ordinate tick mark interval in all panels equals 0.5 absorbance units. The spectra have been shifted vertically for clarity.

tentatively assign it as the ternary combination $\nu_3 + \nu_4 + \nu_8$. It can also be seen in Figure 2 that in the spectra of the AC-d_6 and OX-d_4 complexes a shoulder is present on the low-frequency Fermi component, this time on the high-frequency side: we assign it to the same combination transition, $\nu_3 + \nu_4 + \nu_8$, that causes the 3100 cm^{-1} shoulder in monomer TFE. For the DME-d_6 complex that transition is less clearly visible, but the spectra indicate that it is present as a very weak feature in the high-frequency wing of the 3090.7 cm^{-1} complex band.

Again to avoid excessive overlap, now in the C−D stretching region, the complexes of TFE-d_1 were studied in combination with unlabeled Lewis bases. In Figure 3, the C−D stretching regions of spectra recorded from solutions in LAr, at 95 K, that contain mole fractions of 1.7×10^{-4} of DME and 2.2×10^{-4} of TFE-d_1 (A), and from solutions in LKr, at 143 K, that contain 7.5×10^{-5} of AC and 4.8×10^{-4} of TFE-d_1 (B) and 3.9×10^{-4} of OX-d_4 and 3.1×10^{-4} of TFE-d_1 (C) are compared with those containing only monomers. For the mixed solutions containing DME and OX, a new band due to the C−D stretching fundamental in the complex is observed, red shifted from the monomer transition, by −20.5 and −10.6 cm^{-1}, respectively. Because of the limited solubility of acetone in LKr, and because of the presence of CO_2 as an impurity in the Lewis acid and bases, the analysis for the solutions containing AC and TFE-d_1 is less clear. This is illustrated by the spectra in Figure 3B, where the presence of a band assignable to a complex is not obvious. However, the presence of a weak complex band, red shifted by −5 to −10 cm^{-1}, was detected using subtraction techniques.

The occurrence of a single absorption in the C−D stretching region suggests that in the cryosolutions only one isomer is present for the complexes with both DME and AC.

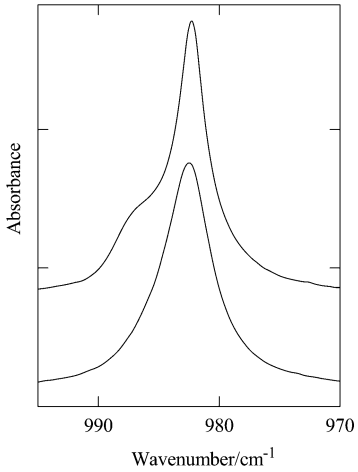

Figure 4. Infrared spectrum in the $\nu_5^{C_2F_3D}$ region of a solution in liquid krypton of trifluoroethene-d_1 and dimethyl ether, at 123 K. The top trace is the spectrum of a mixture of TFE-d_1 and DME; the lower trace, that of a solution of TFE-d_1. The ordinate tick mark interval equals 0.5 absorbance units. The spectra have been shifted vertically for clarity.

The experience with weak complexes observed in liquid rare gases is that, unless the predicted complexation shifts are very small, the ab initio calculations predict the correct directions of the shifts.[13,35] This property can be exploited to identify the observed species in cases where more than one isomer can be formed, given that complexation shifts with opposite directions for different isomers are predicted. In that aspect, the present complexes are not favorable. With one exception, for all vibrational modes of the DME and AC complexes the predicted shifts either are too small or are in the same direction for both isomers. The exception is ν_5 of TFE-d_1, which is predicted to shift +3.9 cm^{-1} in isomer I and −6.4 cm^{-1} in isomer II. In Figure 4 the corresponding regions of the spectra in LKr are shown. With decreasing temperature, a complex band can be seen to emerge on the high-frequency side of monomer ν_5. Using subtraction techniques, the shift was determined to be 4.7 cm^{-1}. It is also evident form Figure 4 that no trace of a complex band can be detected on the low-frequency side. Thus, the observation of a sole, blue-shifted, complex band suggests the conclusion that in the solutions only the planar isomer I is observed. We will see in a later paragraph that other evidence supports this conclusion.

Although it is clear that also with acetone a complex is formed, no evidence for the nature of the observed isomer, similar to that in the previous paragraph, could be found.

Complexation Enthalpies. The standard enthalpies of complexation $\Delta H°$ of the complexes of unlabeled TFE with AC-d_6 and OX-d_4 were determined in LKr, whereas those of the DME-d_6 complexes were determined in LKr and LAr. Typical monomer mole fractions used were in the range between 0.3×10^{-4} and 3.8×10^{-3}, and spectra were recorded at temperatures between 93 and 123 K in LAr, and between 121 and 181 K in LKr. The complexation energies were determined from these spectra using the Van 't Hoff equation. Corrections for temperature variations of the solvent density were applied, as described before.[36] For integration purposes, the spectra of the complexes were isolated by subtracting out rescaled monomer contributions from the spectra of the mixtures. Numerically integrated bands areas were used as integrated intensities.

In Figure 5, typical Van 't Hoff plots obtained for the complexes in LKr are shown. The complexation energies for

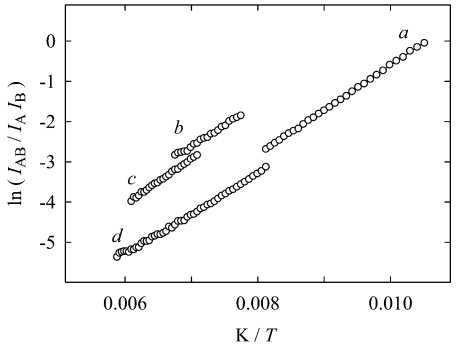

Figure 5. Van't Hoff plots for the determination of the complexation enthalpy of the 1:1 complex of trifluoroethene with dimethyl ether-d_6 in liquid argon (a), and with acetone-d_6 (b), oxirane-d_4 (c), and dimethyl ether-d_6 (d) in liquid krypton.

TABLE 4: Spectral Data Obtained from the Potential and Dipole Surface Calculations for the Fermi Resonance in TFE and Its Complexes with DME-d_6, AC-d_6 and OX-d_4

	TFE	DME(I)	DME(II)	AC(I)	AC(II)	OX
ν_{high}/cm^{-1}	3263	3260	3249	3260	3262	3254
intensity[a]	84	36	41	55	37	53
$\|1,0,0\rangle$[b]	0.740	−0.524	0.702	0.705	0.735	−0.774
$\|0,1,1\rangle$[b]	0.622	0.827	0.664	−0.662	0.625	0.573
ν_{low}/cm^{-1}	3201	3173	3175	3185	3186	3183
intensity[a]	38	66	25	35	18	22
$\|1,0,0\rangle$[b]	−0.594	−0.782	−0.628	−0.627	0.593	0.546
$\|0,1,1\rangle$[b]	0.774	−0.547	0.740	−0.740	−0.771	0.810
R_{calc}	2.2	0.55	1.6	1.6	2.1	2.1
R_{exp}	1.53	0.66/0.71		1.32/1.35		1.32/1.64
ν^o_{high}/cm^{-1}	3240	3237	3220	3231	3235	3232
ν^o_{low}/cm^{-1}	3225	3197	3204	3215	3215	3207
R^o_{calc}	5.0	0.03	1.5	1.7	3.5	10.4

[a] Infrared intensities in km mol^{-1}. [b] Eigenvector elements specifying contribution of the harmonic levels $|1,0,0\rangle$ and $|0,1,1\rangle$ to the components ν_{high} and ν_{low} of the $\nu_1/\nu_2 + \nu_3$ Fermi doublet in TFE.

the solutions in LKr, obtained by averaging the results from two or three independent temperature studies, are −8.8(1) kJ mol^{-1} for TFE·DME-d_6, −10.2(2) kJ mol^{-1} for TFE·AC-d_6, and −10.3(4) kJ mol^{-1} for TFE·OX-d_4. The complexation energy for TFE·DME-d_6 in LAr equals −10.1(1) kJ mol^{-1}.

Discussion

$\nu_1/\nu_2 + \nu_3$ Fermi Resonance. The spectra in Figure 2 reveal that in monomer TFE as well as in the complexes the C−H stretch is involved in a strong Fermi resonance, with the relative intensities of the dyad varying from species to species. The latter are difficult to judge from the spectra because of the presence of the $\nu_3 + \nu_4 + \nu_8$ combination transition, which in all cases overlaps strongly with the low-frequency component of the dyad. The intensity of that component was derived using least squares band fitting, but it is evident that due to the strong overlap the results show a significant uncertainty, and this in turn influences the intensity ratio $R = \nu_{high}/\nu_{low}$ of the dyad. This can be illustrated by comparing the R values obtained by using different profiles in the fitting procedure. The R values derived by using either Gauss/Lorentz sum curves or Voigt profiles have been collected in Table 4, in the row "R_{exp}". Although for monomer TFE and for the AC-d_6 complex both results are rather similar, it can be seen that for the OX-d_4 complex the values differ significantly: the nearly 25% difference presumably is a realistic estimate of the uncertainty for all cases. Anyway, the data in Table 4 show that the strength of the Fermi resonance in the AC-d_6 and OX-d_4 complexes is similar to that in monomer TFE, whereas the inversion of the relative intensity in the DME-d_6 complex signals that in that complex the Fermi resonance is seriously affected by the complexation.

The above observations have been rationalized by anharmonic simulations of the spectra. Although Gaussian03 can calculate cubic and quartic force constants by the finite difference method,[26] it does not produce higher order force constants nor second and higher order dipole derivatives. Therefore, the problem was tackled using ab initio potential and dipole surface calculations. It will be discussed below that, apart from supporting the values of R for monomer TFE and for the AC-d_6 and OX-d_4 complexes, the simulations also lend support to the identification made above of the experimentally observed complex as isomer I.

The model used is based on a three-dimensional approach in which the vibrational potential and the components of the dipole moment of the species is calculated as a function of the dimensionless normal coordinates q_1, q_2, and q_3 for the TFE vibrations of interest, ν_1, ν_2, and ν_3. These coordinates were expressed using the atomic displacements as obtained from ab initio calculations imposing the *very thight* convergence criteria and employing the FREQ = HPMODES option of Gaussian.[27] For each variable a number of equidistant values of the normal coordinate were used. This number was set at 13 for monomer TFE and at 9 for the complexes, the lower number imposed by calculational economy. The values were chosen in an interval sufficiently wide to allow accurate description of the ground and lower excited vibrational states. For each set of values (q_1, q_2, q_3) the Cartesian coordinates of all atoms were derived, and with that geometry the CP-corrected MP/6-31++G(d,p) energy and dipole components were calculated. The resulting 13 × 13 × 13 or 9 × 9 × 9 values for each characteristic were least-squares fit to polynomials of the form

$$V(q_1,q_2,q_3) = \sum_{j=0}^{4}\sum_{k=0}^{4}\sum_{l=0}^{4} c_{jkl}(q_1)^j(q_2)^k(q_3)^l \qquad (1)$$

$$\mu_\alpha(q_1,q_2,q_3) = \sum_{j=0}^{4}\sum_{k=0}^{4}\sum_{l=0}^{4} c^\alpha_{jkl}(q_1)^j(q_2)^k(q_3)^l \qquad (2)$$

with, in all cases, the indices j, k, and l subject to the condition: $j + k + l \le 6$, and with $\alpha = x$, y, or z. Standard deviations of the fit typically were 7.3 × 10^{-5} hartree (16 cm^{-1}) for V, and 1.7 × 10^{-5} debye for μ_α.

The potential $V(q_1,q_2,q_3)$ was used to set up a vibrational Hamiltonian, using triple products of harmonic oscillator functions of the form $\chi_{v1}(q_1)\,\chi_{v2}(q_2)\,\chi_{v3}(q_3)$ as basis functions. The vibrational quantum numbers v_1, v_2, and v_3 varied between 0 and 20, but subject to the restriction $v_1 + v_2 + v_3 \le 20$. The eigenvalues of that 1771 × 1771 Hamiltonian were used to derive the frequencies of the components of the Fermi polyads, and the eigenvectors, combined with the dipole surfaces, eq 2, were used to calculate the corresponding infrared intensities.

The cubic force constant α_{123} that governs the Fermi resonance was calculated from the potential surface to be 76.5 cm^{-1} for monomer TFE. This value is considerable but is consistent with the observed strong equalization of the intensities in the Fermi dyad. To demonstrate the usefulness of the approach, it is of some interest to compare the calculated results for the lower three polyads of monomer TFE with experiment. The necessary data for that have been collected in Table 5. The first column gives the identifiers $|v_1,v_2,v_3\rangle$ of the unperturbed level that contribute most (but not exclusively) to the components of the polyad considered. The experimental relative

TABLE 5: Comparison of Experimental Frequencies and Relative Intensities of Fermi Polyads in Trifluoroethene with Results of Potential and Dipole Surface Calculations

	frequency/cm^{-1}		relative intensity	
assignment	exp	calc	exp	calc
$\|0,1,1\rangle$, $\|1,0,0\rangle$	3107.9	3201	1.0	1.0
	3155.2	3263	1.53/1.49[a]	2.2
	6138.0	6344	1.0	1.0
$\|0,2,2\rangle$, $\|1,1,1\rangle$, $\|2,0,0\rangle$	6207.5	6405	0.25	0.45
	6290.8	6510	0.04	0.05
	9014	9379	1.0	1.0
$\|0,3,3\rangle$, $\|1,2,2\rangle$, $\|2,1,1\rangle$, $\|3,0,0\rangle$		9504		0.09
		9617		0.02
		9761		0.001

[a] Values derived by using Gaus/Lorentz sum curves and Voigt profiles in the least squares band fitting.

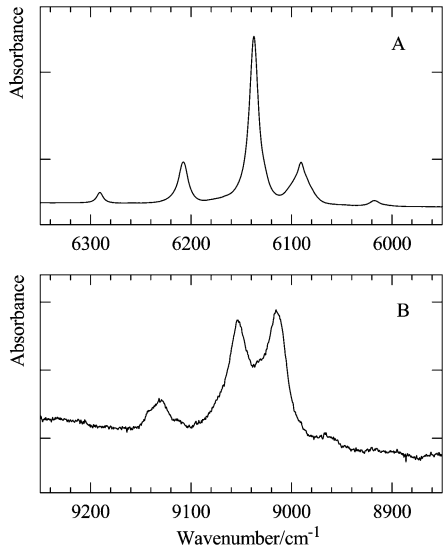

Figure 6. Near-infrared spectra of a solution in liquid krypton at 131 K of trifluoroethene in the region of the first (A) and second (B) overtone $\nu_1/\nu_2 + \nu_3$ Fermi polyads. The ordinate tick mark intervals are 0.2 (A) and 0.05 (B) absorbance units.

intensities, given in the next to last column, and the corresponding calculated values, in the last column, have been normalized to that of the lowest frequency component of each polyad, with the observed values derived using least squares band fitting. The near-infrared spectra of a solution of TFE in liquid krypton, in the regions of the first and second overtones of ν_1, are shown in Figure 6.

It can be seen in Table 5 that in all cases the calculated frequencies are higher than the observed ones, which is the expected result for calculations based on an ab initio potential surface. For the fundamental dyad, the ratio of the observed to the calculated frequency for the low-frequency component is 0.971. When this is applied to the calculated frequency of the other component, a corrected value of 3168.1 cm^{-1} results. This value is in encouraging agreement with the observed frequency of 3155.2 cm^{-1}. It can further be seen that the calculation reproduces the experimental observation that the high-frequency component is the more intense. The calculated I_{high}/I_{low} ratio R of 2.2 must be compared with experimental values of 1.5: in view of the presumably significant uncertainty on the latter (vide supra), the agreement may be termed more than satisfactory.

For the next polyad the calculations predict a triplet with frequencies 6344, 6405 and 6510 cm^{-1}, with decreasing relative intensities. It seems reasonable to assign the first, most intense, component to the band at 6138 cm^{-1}, which, as can be seen in Figure 6A, is the most intense transition in that region. With this assignment, the observed/calculated frequency ratio R equals 0.967, quite similar to that for the fundamental dyad. Applying this correction factor to the frequencies calculated for the second and third component gives values of 6197 and 6299 cm^{-1}, which are very close to the weak transitions observed at 6207.5 and 6290.8 cm^{-1}. This evidently settles the assignments of those two bands. It can be seen in Table 4 that the calculated relative intensities of components 2 and 3 are in quite acceptable agreement with observation.

In the second-overtone polyad, above 9000 cm^{-1}, matters are less self-evident. It can be seen in Table 4 that a quadruplet is predicted, with the lowest component being the most intense and the relative intensity rapidly decreasing for the second to fourth component. The correction factor of the previous polyad applied to the frequency predicted for the lowest transition of the present polyad results in a value of 9074 cm^{-1}. This value is close to the doublet, which can be seen in Figure 6B between 9100 and 9000 cm^{-1}, and which consists of the most intense transitions in this spectral region. When the lower Fermi component is assigned to the high-frequency component of the observed doublet, at 9053 cm^{-1}, the second component is predicted near 9175 cm^{-1}. Table 4 indicates that its predicted intensity is nearly 10% of that of the first component. The signal-to-noise ratio of the observed spectrum is such that a transition with a relative intensity of that order should be clearly visible. In the predicted range, however, no band can be detected. If, instead, the first component is assigned to the lower component of the observed doublet, at 9014 cm^{-1}, the observed/calculated correction factor predicts the second component near 9134 cm^{-1}. Figure 6B reveals that this falls in the range of the weak, strongly overlapping doublet with frequencies of, approximately 9129 and 9143 cm^{-1}. This suggests that it is more likely that the lower component of the Fermi quadruplet must be assigned at 9014 cm^{-1}. Extrapolating the observation that the corrected predicted frequencies of the second and third components of the first-overtone polyad fall slightly below the observed values, we prefer the assignment of the second component of the present polyad to the 9143 cm^{-1} shoulder. Finally, it can be seen that the third and fourth components have predicted intensities that, when compared with the observed intensity of the first component, make them of the same magnitude (third) as, or significantly below (fourth), the noise level of the spectrum. Consistent with this, no bands have been detected in the spectral regions concerned, so that these transitions remain unassigned. All in all it is clear that the simulation calculations produce relevant data for the interpretation of the Fermi resonance in monomer TFE.

The data obtained from the surface calculations for the Fermi dyads in the complexes have been collected in Table 4. Conventional wisdom has it that the component with the highest intensity of a Fermi dyad is closer to the unperturbed fundamental, whereas the component with the lower intensity is closer to the combination band. Using the present simulations, this is easily verified from the eigenvector elements specifying the contributions of the harmonic levels $|1,0,0\rangle$ and $|0,0,1\rangle$. These elements have been included in Table 4. The sum of the squares of these elements for each component of each dyad is between 0.9 and 1.0, showing that the harmonic levels considered indeed are the main contributors to the observed dyad. With the exception of isomer I of TFE·DME-d_6, the experimental values of the intensity ration R_{exp} indicate that the high-frequency component is the more intense. In line with the above expectation, the eigenvector elements for that component in Table 4

show that the contribution of the level $|1,0,0\rangle$ is higher than that of the level $|0,0,1\rangle$. For isomer I of the DME-d_6 complex, where the relative intensity of the dyad is reversed, the largest contribution of the level $|1,0,0\rangle$ is found in the lower component of the dyad.

Next, consider in Table 4 the calculated frequencies and relative intensities in the dyads. It can be seen that for TFE, TFE·AC-d_6, and TFE·OX-d_4 the calculated values of R reproduce the experimental intensity order of the components of the dyad, i.e., the high-frequency one being the more intense. The quantitative agreement leaves somewhat to be desired, but as for monomer TFE, it is not unlikely that this is partly due to the uncertainty on the experimental values resulting from the presence of $\nu_3 + \nu_4 + \nu_8$. This, as is clear from Table 4, indicates the intensity data are not sufficiently accurate to decide between the isomers of TFE·AC-d_6. For TFE·DME-d_6 the calculated values of R reflect opposite intensity orders for the two isomers. The order consistent with experiment is predicted for isomer I, the calculated R, 0.54, to be compared with experimental values of 0.61 and 0.77. The consistency of the calculated results with experiment discussed above justifies the assumption that the intensity predictions for the isomers of TFE·DME-d_6 are qualitatively reliable. The conclusion, therefore, is that the intensity calculations support the presence of isomer I in our solutions.

The data in Table 4 show that the complexation shifts predicted for I are -3 cm^{-1} for the high-frequency component and -28 cm^{-1} for the low-frequency one. This pattern agrees better with experiment, with shifts of -5.8 and -19.3 cm^{-1}, than does that of isomer II, for which the shifts are -14 and -26 cm^{-1}. Thus, the predicted complexation shifts appear to bear out our conclusion based on the value of R.

Another aspect of the above calculations is that the Fermi deperturbed frequencies ν^{o}_{high} and ν^{o}_{low} for the fundamental dyads can be derived. This is achieved by diagonalizing the vibrational Hamiltonian after the value of the coefficient c_{123} of eq 1 has been equated to zero. The complexation shifts derived for these C−H stretches are -28 cm^{-1} (DME(I)) and -20 cm^{-1} (DME(II)), -9 cm^{-1} (AC(I)) and -5 cm^{-1} (AC(II)), and -8 cm^{-1} (OX). All these shifts are toward lower frequencies, which is consistent with the observed red shifts of the C−D stretching in the complexes of TFE-d_1. Also, comparison with the harmonic ab initio shifts in Table 2 shows that the anharmonic corrections do not reverse the directions of the complexation shifts. These data combined are compelling evidence that the hydrogen bond in the present complexes is not of the blue-shifting type.

Complexation Energies. The experimental results obtained in this study immediately raise two problems. The first one is that the evidence collected, even when somewhat indirect, systematically points at the formation of an isomer of TFE·DME, which differs from the one observed in the pulsed beam microwave study.[22] The second problem is the fact that the ab initio calculations predict, as is clear from Table 1, that for DME and AC two isomers of the complex, with nearly identical energies, should exist, whereas for neither Lewis base could experimental evidence for the presence of a second isomer be found.

As to the first problem, it has been shown[37] that the formation/relaxation processes in a molecular beam, such as the one used in the microwave study of TFE·DME,[22] tend to favor the lower energy isomers. Accepting the ab initio near accidental energetic degeneracy of the two isomers, it follows that both isomers should be present in the molecular beam, even if it remains difficult to predict what their relative populations would be, and if the latter would be in line with equilibrium expectations at the vibrational temperature of the beam. The ab initio calculations performed for that study have not revealed the existence of a second isomer, and no mention is made of attempts to detect a second isomer in the beam experiments. Therefore, at least at this stage, our conclusions are not necessarily contradicting the microwave observations.

TABLE 6: Standard Gibbs Energies of Solvation, $\Delta_{sol}G$, in kJ mol^{-1}, Standard Enthalpies of Solvation, $\Delta_{sol}H$, in kJ mol^{-1}, Standard Entropies of Solvation, $\Delta_{sol}S$, in J K^{-1} mol^{-1}, and Solvent Shifts of Standard Gibbs Energies of Complexation, in kJ mol^{-1}, in Liquid Krypton at 151 K[a]

	$\Delta_{sol}G$	$\Delta_{sol}H$	$\Delta_{sol}S$	$\Delta_{sol}(\Delta G°)$
TFE	−8.9(1)	−15.2(1)	−41.4(2)	
DME	−13.7(2)	−23.7(1)	−66.1(6)	
AC	−17.9(2)	−30.9(1)	−86.2(8)	
OX	−13.4(1)	−23.3(1)	−65.7(4)	
TFE·DME(I)	−20.4(2)	−34.7(1)	−95.0(9)	2.2(3)
TFE·DME(II)	−19.3(2)	−32.9(2)	−90.0(14)	3.3(3)
TFE·AC(I)	−23.5(2)	−40.0(2)	−109.3(6)	3.3(3)
TFE·AC(II)	−23.4(2)	−39.6(1)	−107.5(7)	3.4(3)
TFE·OX	−19.1(3)	−32.2(2)	−86.7(17)	3.2(3)

[a] Uncertainties are given in brackets.

Major contributions to the second problem are the solvent effects that influence our experiments but that are absent in the ab initio calculations, and the inherent inaccuracies of the ab initio complexation energies, which are the small differences between the very large total energy of the complex and the also very large sum of total energies of the monomers. Some quantitative insight in these contributions was obtained as follows.

The failure to detect isomer II in our experiments must be the consequence of its concentration being below the detection limit. In view of the signal-to-noise ratio of the spectra, and taking into account that similar infrared intensities are predicted for both isomers, the concentration of II can be set to be not more than 5% of that of isomer I.

Solvent influences on the species in the cryosolutions were obtained from Monte Carlo free energy perturbation theory.[38] For the sake of completeness these calculations were made for all species involved in this study. The results, in the form of Gibbs energies, enthalpies and entropies of solvation, together with the solvent influence on the standard Gibbs energy of complexation, $\Delta_{sol}(\Delta G°) = \Delta G°(\text{LKr}) - \Delta G°(\text{gas})$, are given in Table 6. It can be seen that all $\Delta_{sol}(\Delta G°)$ have positive values between 2.2 and 3.4 kJ mol^{-1}, from which follows that solvation destabilizes the complexes. This is readily rationalized when the loss of solvation required to form the complex is considered.

The solvation enthalpies in Table 6 were used in combination with the ab initio complexation energies in Table 1 to predict the complexation enthalpies in liquid krypton. To that end, the energies are first converted into gas phase complexation enthalpies using zero point and thermal corrections that are easily calculated from the ab intio frequencies and rotation constants.[39] These corrections lower the absolute values of the energies by 2.5−3.5 kJ mol^{-1}, depending on the case. Applying subsequently the solvation enthalpy corrections from Table 6 results in predicted liquid krypton complexation enthalpies of $-9.9(2)$ kJ mol^{-1} (TFE·DME(I)), $-8.3(2)$ and $-7.4(2)$ kJ mol^{-1} (TFE·AC (I) and (II)), and $-11.6(2)$ (TFE·OX). Compared with the experimental values given above, it is clear that the predictions either overestimate (DME, OX) or underestimate (AC) the stabilities of the complexes, by amounts varying between 12 and 27%. Under the assumption that the solvent

corrections are relatively acurate, these deviations trace back to errors on the ab initio complexation energies between, roughly, 1 and 3 kJ mol^{-1}.

For TFE·DME the difference in solvation destabilization between the two isomers is 1.1 kJ mol^{-1} in favor of isomer I; i.e., the relative concentration of isomer I will be higher in solution than in the gas phase. This is a step in the required direction but does not suffice to bring the very small difference in ab initio complexation energy in line with the absence of isomer II in the solutions. It is straightforward to derive from basic thermodynamics a relation for the stability constant K of the complexes of the form

$$\frac{K_s^I/K_s^{II}}{K_g^I/K_g^{II}} = \exp\left[\frac{\Delta_{sol}(\Delta G^*(II) - \Delta_{sol}(\Delta G^*(I))}{RT}\right]$$

with the Roman numerals referring to the isomers, and subscripts s and g to solution and gas phase, respectively. Using the data from Table 6 for TFE·DME, it is found that the ratio of the stability constants, which equals the ratio of the concentrations of the complexes, in liquid krypton is 2.4 times the gas-phase ratio. From this value, and using the 5% upper limit for the concentration of II in LKr, it follows that the gas-phase Gibbs energy of isomer I must be at least 2.7 kJ mol^{-1} lower than that of isomer II. Employing ab initio structures and vibrational frequencies, statistical thermodynamics calculations result in vapor phase standard complexation entropies of −95.1 and −98.1 J K^{-1} mol^{-1} for isomers I and II, respectively. These allow the difference in $\Delta G°$ values to be transformed into a 2.2 kJ mol^{-1} difference of standard complexation enthalpies. Correcting this for zero point and thermal contributions results in a difference between the complexation energies that must be at least 2.2 kJ mol^{-1} in favor of isomer I. This is significantly higher than the 0.1 kJ mol^{-1} derived in the basis set limit, Table 1. Thus, the absence of isomer II from our solutions proves that the ab initio energies cannot be very accurate. If the difference is evenly divided over the two isomers, each complexation energy must be off by at least 1.6 kJ mol^{-1}. This error is consistent with those estimated in the previous paragraph and is of the same magnitude as that of previous estimates of complexation energies of similar weak complexes.[15,35] The conclusion must be that ab initio complexation energies at the level used here can be anticipated to show an uncertainty on the order of 10−20%.

Conclusions

In this study the formation of 1:1 complexes of TFE with DME, AC, and OX has been observed in cryogenic solutions, using liquid argon and liquid krypton as solvents. Analysis of the infrared spectra of the solutions shows that for all Lewis bases a complex with the Lewis acid is formed. Ab initio calculations show that the interaction between Lewis base and Lewis acid occurs via, primarily, a hydrogen bond between the TFE C−H bond and the oxygen atom of the Lewis base, with secondary interactions between the methyl or methylene C−H bonds and fluorine atoms of the Lewis acid.

For the complexes of DME and AC, two different isomers of the 1:1 complex are predicted, one with the heavy atom planes of both monomers in the same plane, the other with these planes at right angles. The isomers are predicted to have very nearly the same energies. Comparison of the experimental with the ab initio vibrational frequencies suggests that for DME the complex with the planar heavy atom skeleton is formed in the solutions, at variance with literature microwave results on the same complex.

The Fermi resonance between the ν_1 and $\nu_2 + \nu_3$ levels of TFE was investigated in the monomer as well as in the complexes using potential and dipole hypersurfaces calculated by ab initio methods. The results thereof show that the hydrogen bond in the complexes is of the traditional, red-shifting type, substantiating the conclusion derived from the spectra of the complexes of TFE-d_1 with the same Lewis bases. The hypersurface calculations further confirm the nature of the TFE·DME complex as derived from the complexation shifts.

The complexation enthalpies of the complexes were determined to be rather similar, with values falling between −8.8(1) (DME) and −10.3(4) kJ mol^{-1} (OX). Monte Carlo calculations on the solvation influences show that the complexes are less stable in solution than in the vapor phase, and a critical analysis of the data allows us to estimate the uncertainty on the ab initio complexation energies in the Complete Basis Limit to be on the order of 1−3 kJ mol^{-1}.

Acknowledgment. Gratitute is expressed to the FWO-Vlaanderen for their assistance toward the purchase of spectroscopic equipment used in this study. We thank the Flemish Community for financial support through the Special Research Fund.

References and Notes

(1) Alabugin, I. V.; Manoharan, M.; Peabody, S.; Weinhold, F. *J. Am. Chem. Soc.* **2003**, *125*, 5973.
(2) Barnes, A. J. *J. Mol. Struct.* **2004**, *704*, 3.
(3) Castellano, R. K. *Curr. Org. Chem.* **2004**, *8*, 845.
(4) Desiraju, G. R. *Chem. Commun.* **2005**, 2995.
(5) Hermansson, K. *J. Phys. Chem. A* **2002**, *106*, 4695.
(6) Hobza, P.; Havlas, Z. *Theor. Chem. Acc.* **2002**, *108*, 325.
(7) Li, X. S.; Liu, L.; Schlegel, H. B. *J. Am. Chem. Soc.* **2002**, *124*, 9639.
(8) Pejov, L.; Hermansson, K. *J. Chem. Phys.* **2003**, *119*, 313.
(9) Scheiner, S.; Kar, T. *J. Phys. Chem. A* **2002**, *106*, 1784.
(10) Wang, J. T.; Feng, Y.; Liu, L.; Li, X. S.; Guo, Q. X. *Chem. Lett.* **2003**, *32*, 746.
(11) Zierkiewicz, W.; Jurecka, P.; Hobza, P. *Chemphyschem* **2005**, *6*, 609.
(12) Hobza, P.; Havlas, Z. *Chem. Rev.* **2000**, *100*, 4253.
(13) Delanoye, S. N.; Herrebout, W. A.; Van der Veken, B. J. *J. Am. Chem. Soc.* **2002**, *124*, 11854.
(14) Delanoye, S. N.; Herrebout, W. A.; Van der Veken, B. J. *J. Am. Chem. Soc.* **2002**, *124*, 7490.
(15) Delanoye, S. N.; Herrebout, W. A.; Van der Veken, B. J. *J. Phys. Chem. A* **2005**, *109*, 9836.
(16) Herrebout, W. A.; Delanoye, S. N.; van der Veken, B. J. *J. Phys. Chem. A* **2004**, *108*, 6059.
(17) Alonso, J. L.; Antolinez, S.; Blanco, S.; Lesarri, A.; Lopez, J. C.; Caminati, W. *J. Am. Chem. Soc.* **2004**, *126*, 3244.
(18) Jeng, M. L. H.; Ault, B. S. *J. Phys. Chem.* **1990**, *94*, 4851.
(19) Scheiner, S.; Grabowski, S. J.; Kar, T. *J. Phys. Chem. A* **2001**, *105*, 10607.
(20) Mann, D. E.; Acquista, N.; Plyler, E. K. *J. Chem. Phys.* **1954**, *22*, 1586.
(21) McKean, D. C. *Spectrochim. Acta A* **1975**, *31*, 1167.
(22) Tatamitani, Y.; Ogata, T. *J. Mol. Spectrosc.* **2003**, *222*, 102.
(23) Hartgraves, G. A.; Burton, D. J. *J. Fluorine Chem.* **1988**, *39*, 425.
(24) Van der Veken, B. J.; Demunck, F. R. *J. Chem. Phys.* **1992**, *97*, 3060.
(25) Simon, S.; Duran, M.; Dannenberg, J. J. *J. Chem. Phys.* **1996**, *105*, 11024.
(26) Barone, V. *J. Chem. Phys.* **2005**, *122*.
(27) Frisch, M. J.; Trucks, G. W.; Schlegel, H. B.; Scuseria, G. E.; Robb, M. A.; Cheeseman, J. R.; Montgomery, J. A., Jr.; Vreven, T.; Kudin, K. N.; Burant, J. C.; Millam, J. M.; Iyengar, S. S.; Tomasi, J.; Barone, V.; Mennucci, B.; Cossi, M.; Scalmani, G.; Rega, N.; Petersson, G. A.; Nakatsuji, H.; Hada, M.; Ehara, M.; Toyota, K.; Fukuda, R.; Hasegawa, J.; Ishida, M.; Nakajima, T.; Honda, Y.; Kitao, O.; Nakai, H.; Klene, M.; Li, X.; Knox, J. E.; Hratchian, H. P.; Cross, J. B.; Bakken, V.; Adamo, C.; Jaramillo, J.; Gomperts, R.; Stratmann, R. E.; Yazyev, O.; Austin, A. J.; Cammi, R.; Pomelli, C.; Ochterski, J. W.; Ayala, P. Y.; Morokuma, K.; Voth, G. A.; Salvador, P.; Dannenberg, J. J.; Zakrzewski, V. G.; Dapprich, S.; Daniels, A. D.; Strain, M. C.; Farkas, O.; Malick, D. K.; Rabuck, A. D.; Raghavachari, K.; Foresman, J. B.; Ortiz, J. V.; Cui, Q.; Baboul, A.

G.; Clifford, S.; Cioslowski, J.; Stefanov, B. B.; Liu, G.; Liashenko, A.; Piskorz, P.; Komaromi, I.; Martin, R. L.; Fox, D. J.; Keith, T.; Al-Laham, M. A.; Peng, C. Y.; Nanayakkara, A.; Challacombe, M.; Gill, P. M. W.; Johnson, B.; Chen, W.; Wong, M. W.; Gonzalez, C.; Pople, J. A. *Gaussian 03*, revision A.5; Gaussian, Inc.: Wallingford, CT, 2004.

(28) Ishimura, K.; Pulay, P.; Nagase, S. *J. Comput. Chem.* **2006**, *27*, 407.

(29) *PQS*, version 3.1; Parallel Quantum Solutions: 203 Green Acres Rd., Fayetteville, AR 72703, 2005.

(30) Biegler-Konig, F.; Schonbohm, J.; Bayles, D. *J. Comput. Chem.* **2001**, *22*, 545.

(31) Jorgensen, W. L. *BOSS*, version 4.1; Yale University: New Haven, CT, 1999.

(32) Van Ginderen, P.; Herrebout, W. A.; van der Veken, B. J. *J. Phys. Chem. A* **2003**, *107*, 5391.

(33) Herrebout, W. A.; Melikova, S. M.; Delanoye, S. N.; Rutkowski, K. S.; Shchepkin, D. N.; Van der Veken, B. J. *J. Phys. Chem. A* **2005**, *109*, 3038.

(34) Van den Kerkhof, T.; Bouwen, A.; Goovaerts, E.; Herrebout, W. A.; Van der Veken, B. J. *Phys. Chem. Chem. Phys.* **2004**, *6*, 358.

(35) Everaert, G. P.; Herrebout, W. A.; van der Veken, B. J. *Spectrochim. Acta A* **2005**, *61*, 1375.

(36) Van der Veken, B. J. *J. Phys. Chem.* **1996**, *100*, 17436.

(37) Ruoff, R. S.; Klots, T. D.; Emilsson, T.; Gutowsky, H. S. *J. Chem. Phys.* **1990**, *93*, 3142.

(38) Jorgensen, W. L. *BOSS 4.1*, version 4.1 ed.; Yale University: New Haven, CT, 1999.

(39) McQuarrie, D. A. *Statistical Mechanics*; University Science Books: Sausalito, CA, 2000.